May 1989 LIDS-P-1875

# SIMULTANEOUS INVERSION OF VELOCITY AND DENSITY PROFILES

by

**Ali Ozbek**
Department of Electrical Engineering and Computer Science
and
Earth Resources Laboratory
Massachusetts Institute of Technology
Cambridge, MA 02139

**Bernard C. Levy**
Department of Electrical Engineering and Computer Science
University of California
Davis, CA 95616

This work was supported by the Air Force Office of Scientific Research under Grant No. AFOSR-85-0227, by the National Science Foundation under Grant No. ECS-83-12921, and by the Vertical Seismic Profiling Consortium at the MIT Earth Resources Laboratory.

# Simultaneous Inversion of Velocity and Density Profiles



*Ali Özbek, M.I.T.; and Bernard C. Levy, University of California at Davis*


## Summary

The multidimensional inverse scattering problem for an acoustic medium is considered within the homogeneous background Born approximation. The objective is to reconstruct simultaneously the velocity and density profiles of the medium. The medium is probed by wide-band plane-wave sources, and the time traces observed at the receivers are appropriately filtered to obtain generalized projections of the velocity and density scattering potentials, which are related to the velocity and density variations in the medium. The generalized projections are weighted integrals of the scattering potentials; in the two-dimensional geometry the weighting functions are concentrated along parabolas. The reconstruction problem for the generalized projections is formulated in a way similar to the problem of x-ray, or straight-line tomography. The solution is expressed as a backprojection operation followed by a two dimensional space-invariant filtering operation. In the Fourier domain, the resulting image is a linear combination of the velocity and density scattering potentials, where the coefficients depend on the angle of incidence of the probing wave. Therefore, two or more different angles of incidence are necessary to solve for the velocity and density scattering potentials separately.

The technique of defining a backprojection operator and relating it to the unknown medium for the case of zero-offset problems, where projections over circles arise, was introduced by Fawcett (1985). With a similar technique, Özbek & Levy (1987) solved the velocity inversion problem in constant-density acoustic media under plane-wave illumination, where parabolic projections are the data. This work extends this work to the joint reconstruction of velocity and density. Only the 2D case is presented here, for the 3D case and more detailed development, see Özbek & Levy (1988). The extension of these results to the elastic problem, where elliptic and hyperbolic, as well as parabolic projections are inverted, will be presented elsewhere.


## Introduction

Consider the scattering experiment described in Fig. 1. A 2-D acoustic medium is probed by a wide-band plane wave and the scattered field is observed along a straight-line receiver array. The pressure field $P(\underline{x},\omega)$ at position $\underline{x}=(x,y)$ satisfies

$$\rho(\underline{x})\nabla\cdot\left[\frac{1}{\rho(\underline{x})}\nabla P(\underline{x},\omega)\right]+\frac{\omega^2}{c^2(\underline{x})}P(\underline{x},\omega)=0, \tag{1}$$

where $c(\underline{x})$ is the propagation velocity, and $\rho(\underline{x})$ is the density of the medium at point $\underline{x}$. Within the Born approximation, the scattered field $P_s(\underline{\xi},\omega)$ at receiver location $\underline{\xi}$ can then be written as

$$\begin{aligned}P_s(\underline{\xi},\omega) &= \int d\underline{x}'\left\{k^2[U_c(\underline{x}')-U_\rho(\underline{x}')]P_o(\underline{x}',\omega)G_o(\underline{\xi},\underline{x}',\omega)\right.\\ &\left.+U_\rho(\underline{x}')\nabla_{\underline{x}'}P_o(\underline{x}',\omega)\cdot\nabla_{\underline{x}'}G_o(\underline{\xi},\underline{x}',\omega)\right\}, \end{aligned}\tag{2}$$

where $k=\omega/c_o$ is the wavenumber. The scattered field $P_s$ is the difference between the total field $P$ and the incident field $P_o$. $G_o$ is the Green's function associated with a point source in a homogeneous medium. $U_c(\underline{x})\triangleq[c_o^2/c^2(\underline{x})]-1$ and $U_\rho(\underline{x})\triangleq\ln[\rho(\underline{x})/\rho_o]$ can be termed the "velocity scattering potential" and the "density scattering potential", respectively. $c_o$ is the propagation velocity, and $\rho_o$ is the density of the background medium. We assume that $c(\underline{x})$ and $\rho(\underline{x})$ do not deviate significantly from the background values of $c_o$ and $\rho_o$; consequently the $U_c(\underline{x})$ and $U_\rho(\underline{x})$ values are small with respect to 1. We also assume that $U_c(\underline{x})$ and $U_\rho(\underline{x})$ have the bounded support $\mathcal{V}$, which is disconnected from the receiver array.

From (2), it can be deduced that the scattering pattern due to $U_c(\underline{x})$ is that of a monopole, whereas the scattering pattern due to $U_\rho(\underline{x})$ is that of the sum of a monopole and a dipole. Therefore, the scattering due to density perturbations is most prominent for reflected waves, and the least prominent for reflected ones.

The incident wave is given as $P_o(\underline{x}',\omega)=e^{ik\hat{\underline{\theta}}\cdot\underline{x}'}$, where $\hat{\underline{\theta}}=(\cos\theta,\ \sin\theta)$ is the unit vector which indicates the angle of incidence of the plane-wave source. For the 2-D geometry, the Green's function is given as $G_o(\underline{x},\underline{x}',\omega)=i\mathrm{H}_0^{(1)}(k|\underline{x}-\underline{x}'|)/4$, where $\mathrm{H}_0^{(1)}(\cdot)$ indicates the Hankel function of order zero and type one.

We now now filter the observed scattered field:

$$\hat{g}(\xi,k_r)\triangleq\frac{2\pi}{k_r^2}P_s^*(\underline{\xi},c_ok_r). \tag{3}$$

From (2), the inverse Fourier transform of $\hat{g}(\xi,k_r)$ with respect to $k_r$ can be written as

$$g(\xi,r)=\int d\underline{x}'\frac{1(r-\hat{\underline{\theta}}\cdot\underline{x}'-|\underline{x}'-\underline{\xi}|)}{\sqrt{(r-\hat{\underline{\theta}}\cdot\underline{x}')^2-|\underline{x}'-\underline{\xi}|^2}}$$

$$\left\{[U_c(\underline{x}')-U_\rho(\underline{x}')]-\left[\hat{\underline{\theta}}\cdot\frac{(\underline{x}'-\underline{\xi})}{|\underline{x}'-\underline{\xi}|}\right]\left[\frac{r-\hat{\underline{\theta}}\cdot\underline{x}'}{|\underline{x}'-\underline{\xi}|}\right]U_\rho(\underline{x}')\right\}. \tag{4}$$

This equation expresses $g(\xi,r)$ as a weighted integral of scattering potentials $U_c(\underline{x})$ and $U_\rho(\underline{x})$, where the weighting function is nonzero in a region with parabolic support. In the following, it will be assumed that the projections $g(\xi,r)$ constitute the data that is given by the scattering experiment. Therefore, the inverse scattering problem can be formulated as follows: given the generalized projections $\{g(\xi,r):\ -\infty<\xi<\infty,\ 0\le r<\infty\}$, we want to reconstruct the scattering potentials $U_c(\underline{x})$ and $U_\rho(\underline{x})$.

It is interesting to note that the parabolical projections $g(\xi,r)$ can be obtained in the time domain also:

$$\begin{aligned}g(\xi,r) &= -2\pi c_o\int_{-\infty}^{r/c_o}d\tau\int_{-\infty}^{\tau}ds P_s(\underline{\xi},s)\\ &\quad+4\pi^2c_o\int_{-\infty}^{\infty}d\tau\int_{-\infty}^{\tau}dsP_s(\underline{\xi},s).\end{aligned} \tag{5}$$

## The Backprojection Operation

The first step of our inversion procedure is to perform a backprojection operation on the projections $g(\xi,r)$. We define it as

$$U_B(\underline{x}) \triangleq \int_{-\infty}^{\infty} d\xi \int_{-\infty}^{\infty} dr g(\xi, r) \frac{1(r - \underline{\hat{\theta}} \cdot \underline{x} - |\underline{x} - \underline{\xi}|)}{\sqrt{(r - \underline{\hat{\theta}} \cdot \underline{x})^2 - |\underline{x} - \underline{\xi}|^2}}. \quad (6)$$

At a given point $\underline{x}$, this operation sums the contributions of the projections $g(\xi, r)$ which correspond to scattering equation (4). By performing this backprojection operation for every point in the plane, this gives an image, $U_B(\underline{x})$.

Our first objective is to relate $g(\xi, r)$ and $U_B(\underline{x})$ in the frequency domain. It can be shown that the Fourier transform of $U_B(\underline{x})$ is given by (Özbek & Levy (1987))

$$\hat{U}_B(\underline{k}) = \frac{i\pi}{\underline{k} \cdot \underline{\hat{\theta}}} e^{-ip\underline{\lambda} \cdot \underline{\hat{\psi}}/2\underline{k} \cdot \underline{\hat{\theta}}} \hat{g}\left(k_\xi = \frac{\underline{\lambda} \cdot \underline{\hat{\psi}}^\perp}{2\underline{k} \cdot \underline{\hat{\theta}}},\ k_r = \frac{k^2}{2\underline{k} \cdot \underline{\hat{\theta}}}\right), \quad (7)$$

where $\hat{g}(k_\xi, k_r)$ is the 2-D Fourier transform of $g(\xi, r)$, $\underline{k} = (k_x, k_y)$, $k = |\underline{k}|$, $\underline{\lambda} = (k_x^2 - k_y^2,\ 2k_xk_y)$, $\underline{\hat{\psi}} = (\cos(\theta + \phi),\ \sin(\theta + \phi))$, and $\underline{\hat{\psi}}^\perp = (\sin(\theta + \phi),\ -\cos(\theta + \phi))$.

## Separate Reconstruction of $\hat{U}_c(\underline{k})$ and $\hat{U}_\rho(\underline{k})$

In this section, we first derive a frequency domain relationship between the projections $g(\xi, r)$ and the scattering potentials $U_c(\underline{x})$ and $U_\rho(\underline{x})$, thus obtaining a "Projection Slice Theorem" associated with the problem. Inverting this relationship provides both a frequency domain relationship between $\hat{U}_c(\underline{k})$, $\hat{U}_\rho(\underline{k})$, and $\hat{U}_B(\underline{k})$, and a method for the separate reconstruction of $U_c(\underline{x})$ and $U_\rho(\underline{x})$.

From (2) and (3), we obtain (Özbek & Levy (1988))

$$\hat{g}(k_\xi, k_r) = -\frac{i\pi\gamma}{\Sigma} e^{ip\Sigma} \left\{ (\hat{U}_c - \hat{U}_\rho)(\underline{k} = k_r\underline{\hat{\theta}} + k_\xi\underline{\hat{\phi}}^\perp + \Sigma\underline{\hat{\phi}}) - \frac{\underline{\hat{\theta}} \cdot [k_\xi\underline{\hat{\phi}}^\perp + \Sigma\underline{\hat{\phi}}]}{k_r} \hat{U}_\rho(\underline{k} = k_r\underline{\hat{\theta}} + k_\xi\underline{\hat{\phi}}^\perp + \Sigma\underline{\hat{\phi}}) \right\}, \quad (8)$$

for $|k_\xi| \le |k_r|$, where $\hat{U}_c(\underline{k})$ and $\hat{U}_\rho(\underline{k})$ are the 2-D Fourier transforms of $U_c(\underline{x})$ and $U_\rho(\underline{x})$ respectively, $\Sigma \triangleq \gamma\text{sgn}(k_r)\sqrt{k_r^2 - k_\xi^2}$, and

$$\gamma \triangleq \begin{cases} +1 & \text{if } \underline{x} \cdot \underline{\hat{\phi}} - p > 0 \text{ for all } \underline{x} \in \mathcal{V}, \\ -1 & \text{if } \underline{x} \cdot \underline{\hat{\phi}} - p < 0 \text{ for all } \underline{x} \in \mathcal{V}. \end{cases}$$

For $|k_\xi| > |k_r|$, $\hat{g}(k_\xi, k_r)$ is related to the part of the observed scattered field that corresponds to evanescent waves (Özbek & Levy (1987)), and we do not make use of this portion of $\hat{g}(k_\xi, k_r)$ in our inversion scheme . The inverse formula of (8) is

$$\begin{aligned} \hat{U}_R(\underline{k}) &\triangleq \hat{U}_c(\underline{k}) - 2\left[\frac{(\underline{k} \cdot \underline{\hat{\theta}})^2}{k^2}\right] \hat{U}_\rho(\underline{k}) \quad (9) \\ &= \frac{i\gamma\underline{\lambda} \cdot \underline{\hat{\psi}}}{2\pi\underline{k} \cdot \underline{\hat{\theta}}} e^{-ip\underline{\lambda} \cdot \underline{\hat{\psi}}/2\underline{k} \cdot \underline{\hat{\theta}}} \hat{g}\left(k_\xi = \frac{\underline{\lambda} \cdot \underline{\hat{\psi}}^\perp}{2\underline{k} \cdot \underline{\hat{\theta}}},\ k_r = \frac{k^2}{2\underline{k} \cdot \underline{\hat{\theta}}}\right), \end{aligned}$$

for $\underline{k} \in C$, where the cone $C$ is defined below. $\hat{U}_R(\underline{k})$ denotes the 2-D Fourier transform of the reconstructed potential $U_R(\underline{x})$ which is obtained by applying the constant density reconstruction procedure to the projections $g(\xi, r)$ obtained from a variable density and velocity medium.

Equation (8) represents the "Projection Slice Theorem" associated with the variable density inverse acoustic problem relating the 1-D Fourier transform of $\hat{g}(\xi, k_r)$ with respect to $\xi$ to a semicircular slice of the 2-D Fourier transform of $U_R(\underline{x})$. For a fixed $k_r$, $\hat{g}(k_\xi, k_r)$ gives $\hat{U}_R(\underline{k})$ along a semicircle of radius $|k_r|$ centered at $k_r\underline{\hat{\theta}}$. By letting $k_r$ vary, these semicircles span a cone $C$, which is defined as

$$C = \{\underline{k} :\ |\underline{\hat{k}} \cdot \underline{\hat{\nu}}| \ge \sqrt{2}/2\} \quad (10)$$

for $\gamma = +1$, where $\underline{k} = (\underline{\hat{k}}, k)$ and $\underline{\hat{\nu}} = (\cos(\theta+\phi)/2,\ \sin(\theta+\phi)/2)$. The angular range of this cone is 90°. For $\gamma = -1$, $C$ is the complement $\bar{C}$ of the above cone.

Combining (7) and (9) gives

$$\hat{U}_R(\underline{k}) = \frac{\gamma\underline{\lambda} \cdot \underline{\hat{\psi}}}{2\pi^2} \hat{U}_B(\underline{k}) = \hat{U}_c(\underline{k}) - 2\cos^2\varsigma\, \hat{U}_\rho(\underline{k}), \quad \underline{k} \in C. \quad (11)$$

where $\varsigma$ is the angle between the vectors $\underline{\hat{k}}$ and $\underline{\hat{\theta}}$, with $\underline{k} = (\underline{\hat{k}}, k)$. This relation shows that $\hat{U}_R(\underline{k})$ can be computed by two-dimensional filtering of the backprojected image $\hat{U}_B(\underline{k})$, but then since $\hat{U}_R(\underline{k})$ is a linear combination of $\hat{U}_c(\underline{k})$ and $\hat{U}_\rho(\underline{k})$ we cannot reconstruct these two potentials separately from a single experiment. Therefore, to reconstruct $\hat{U}_c(\underline{k})$ and $\hat{U}_\rho(\underline{k})$ separately, in principle we need two experiments with plane waves incident at angles $\underline{\hat{\theta}}_1$ and $\underline{\hat{\theta}}_2$; then we can solve the system

$$\underbrace{\begin{bmatrix} 1 & -2(\underline{\hat{k}} \cdot \underline{\hat{\theta}}_1)^2 \\ 1 & -2(\underline{\hat{k}} \cdot \underline{\hat{\theta}}_2)^2 \end{bmatrix}}_{M(\underline{\hat{k}}; \underline{\hat{\theta}}_1, \underline{\hat{\theta}}_2)} \begin{bmatrix} \hat{U}_c(\underline{k}) \\ \hat{U}_\rho(\underline{k}) \end{bmatrix} = \begin{bmatrix} \hat{U}_{R1}(\underline{k}) \\ \hat{U}_{R2}(\underline{k}) \end{bmatrix}, \quad (12)$$

which requires inverting the matrix $M(\underline{\hat{k}}; \underline{\hat{\theta}}_1, \underline{\hat{\theta}}_2)$.

For the numerical stability and robustness of the matrix inversion procedure, the matrix $M(\underline{\hat{k}}; \underline{\hat{\theta}}_1, \underline{\hat{\theta}}_2)$ must be as nonsingular as possible. The most appropriate measure of the singularity of a matrix is the smallest singular value of the matrix. Inversion of $M$ would be most robust when the smallest singular value $\sigma_{\min}(M)$ is maximized. This takes place for values of $\underline{\hat{k}}$, $\underline{\hat{\theta}}_1$, and $\underline{\hat{\theta}}_2$ such that $\underline{\hat{\theta}}_1 \cdot \underline{\hat{\theta}}_2 = 0$ and $\underline{\hat{k}} = \pm\underline{\hat{\theta}}_1$ or $\underline{\hat{k}} = \pm\underline{\hat{\theta}}_2$. Therefore the two probing waves are incident at angles perpendicular to each other. Under this condition, let us consider the frequency domain coverage we would have for finite bandwidth data, assuming that we have receiver coverage surrounding the medium. Neglecting the low frequency cutoff band, the frequency domain coverage due to a single probing wave has a "figure-of-eight" shape aligned with the direction of the probing wave (Özbek & Levy (1987)). When two probing waves are used, $U_c(\underline{k})$ and $U_\rho(\underline{k})$ can be solved only in regions where where there is double coverage, as indicated by shaded areas in Fig. 2. However, if we consider the superimposed "radiation pattern" of $\sigma_{\min}(M)$ drawn in Fig. 2 also, we see that $M$ is most singular for those values of $\underline{k}$ where we have double coverage.

For general values of $\underline{\hat{\theta}}_1$ and $\underline{\hat{\theta}}_2$ the situation is similar. In general, $M$ is singular for values of $\underline{\hat{k}}$ which satisfy $|\underline{\hat{k}} \cdot \underline{\hat{\theta}}_1| = |\underline{\hat{k}} \cdot \underline{\hat{\theta}}_2|$. Therefore, for $\underline{\hat{\theta}}_1 = \pm\underline{\hat{\theta}}_2$, $M$ is singular for all $\underline{\hat{k}}$; otherwise, it is singular for $\underline{\hat{k}} = \pm(\underline{\hat{\theta}}_1 + \underline{\hat{\theta}}_2)/|\underline{\hat{\theta}}_1 + \underline{\hat{\theta}}_2|$ or $\underline{\hat{k}} = \pm(\underline{\hat{\theta}}_1 - \underline{\hat{\theta}}_2)/|\underline{\hat{\theta}}_1 - \underline{\hat{\theta}}_2|$. These are the directions which in fact bisect the regions where there is double coverage.

In practice, then, it would be appropriate to use more than two angles, say angles $\underline{\hat{\theta}}_1, \underline{\hat{\theta}}_2, \ldots, \underline{\hat{\theta}}_N$, and for each $\underline{k}$, solve the resulting system

$$\underbrace{\begin{bmatrix} 1 & -2(\underline{\hat{k}} \cdot \underline{\hat{\theta}}_{i_{\underline{k}1}})^2 \\ 1 & -2(\underline{\hat{k}} \cdot \underline{\hat{\theta}}_{i_{\underline{k}2}})^2 \\ \vdots & \vdots \\ 1 & -2(\underline{\hat{k}} \cdot \underline{\hat{\theta}}_{i_{\underline{k}P}})^2 \end{bmatrix}}_{M(\underline{k})} \begin{bmatrix} \hat{U}_c(\underline{k}) \\ \hat{U}_\rho(\underline{k}) \end{bmatrix} = \underbrace{\begin{bmatrix} \hat{U}_{Ri_{\underline{k}1}}(\underline{k}) \\ \hat{U}_{Ri_{\underline{k}2}}(\underline{k}) \\ \vdots \\ \hat{U}_{Ri_{\underline{k}P}}(\underline{k}) \end{bmatrix}}_{\underline{d}_R(\underline{k})} \quad (13)$$

by the least squares method, where $\{i_{\underline{k}1}, i_{\underline{k}2}, \ldots, i_{\underline{k}P}\} \subset \{1, 2, \ldots, N\}$ is the set of indices corresponding to the angles of incidence for which the probing wave provides coverage at $\underline{k}$. This gives the solution

$$\begin{bmatrix} \hat{U}_c(\underline{k}) \\ \hat{U}_\rho(\underline{k}) \end{bmatrix} = (M'M)^{-1}M'\,\underline{d}_R(\underline{k}). \tag{14}$$

## Numerical Example

The theory presented in this paper was tested for the two-dimensional case, using computer-generated synthetic data. Figs. 3a and 3b show the velocity and density scattering potential models, $U_c(\underline{x})$ and $U_\rho(\underline{x})$, respectively. The scattering potentials correspond to velocity and density anomalies which are constant in square-shaped areas of dimensions 35 m × 35 m. The background medium was homogeneous with velocity 5000 m/s. The source wavelet was lowpass with a cutoff frequency of 425 Hz, so that the object sizes are three times the shortest wavelength in the source signal. The regions of anomaly are separated by a distance six times the shortest wavelength. The synthetic scattered waves were obtained by using the forward scattering equation under Born approximation; however, since the object sizes were not too large with respect to the shortest wavelength, we do not deem this approximation to be critical for this example, for small scattering potential magnitudes. The entire image area was 500 m × 500 m, the grid size was 5 m × 5 m, and receivers were located on all sides around the medium, 100 on each side.

As indicated above, for numerical stability in the individual reconstruction of velocity and density inhomogeneities, more than two sources are needed. In this experiment, we have used eight angles of incidence, at 22.5° intervals. The inversion was performed over the regions in the $\underline{k}$ domain where coverage was provided by at least five probing waves; i.e., using the notation of eq. (14), $N = 8$, $P \geq 5$, and rank$(M) \geq 4$ for all inversion points $\underline{k}$. This corresponds to carrying out the inversion over a circular lowpass region with a radius of about 55% of the maximum frequency coverage provided by a single source.

For comparison, we first present the images $U_B(\underline{x})$ and $U_R(\underline{x})$. To obtain these images, in the frequency domain, values obtained due to different sources providing multiple coverage were simply averaged point by point. Fig. 4 shows the backprojected image $U_B(\underline{x})$. $U_B(\underline{x})$ can be interpreted as a "migrated" image of the velocity field for a constant density medium. Fig. 5 depicts $U_R(\underline{x})$, which is the image obtained by applying the constant density reconstruction procedure to the data obtained from a variable density and velocity medium.

Some observations can be made regarding these images. Both images display the locations of the scatterers; however the "inversion" image looks much better focused than the "migration" image. This effect in general has been noted by other researchers also (Esmersoy & Miller (1987)). In addition, the values of $U_B(\underline{x})$ are orders of magnitude different than the original scattering potential levels. On the other hand, $U_R(\underline{x})$ looks like $U_c(\underline{x}) - U_\rho(\underline{x})$, and actual constructed values confirm this. To see how this comes about, consider that our averaging scheme in the frequency domain can be ideally written as

$$\hat{U}_T(\underline{k}) = \frac{1}{\pi}\int_0^\pi d\theta\,\hat{U}_R(\underline{k}) = \hat{U}_c(\underline{k}) - \hat{U}_\rho(\underline{k}), \tag{15}$$

using eqn. (9), where $\hat{U}_R$ corresponds to the inversion result for one source, and $\hat{U}_T$ corresponds to the result after averaging. Therefore, what we have actually obtained this way is the scattering potential associated with the compressibility of the medium.

Figs. 6a and 6b show the separate reconstructions of $U_c(\underline{x})$ and $U_\rho(\underline{x})$, respectively. The numerical values obtained are within 20% of the model values. The sources of error are the bilinear interpolation used, the finite size of receiver arrays on each side, lowpass nature of the frequency domain coverage, the source deconvolution process, and the lack of zero frequency information.

In fact, the the scattered field $P_s(\underline{\xi}, \omega)$ has zero amplitude for zero frequency, as one can observe from the Lippmann-Schwinger equation. In addition, the coefficient of $\hat{U}_\rho(\underline{k})$ in eqn. (9) is not analytic around $\underline{k} = \underline{0}$. Therefore, the DC level cannot be reconstructed with the derived inversion formulas. In our implementation, we have instead estimated it from the closest eight values, arbitrarily assigning a weight of 1/6 to the closest four samples, and 1/12 to the next closest samples which are diagonally located.

## Conclusions

We considered the problem of the separate reconstruction of the velocity and density inhomogeneities for a multidimensional acoustic medium probed by wide-band plane waves. The problem was posed as a generalized tomographic problem, where weighted integrals of the velocity scattering potential $U_c(\underline{x})$ and the density scattering potential $U_\rho(\underline{x})$ are considered as data. A backprojection operator $U_B(\underline{x})$ was defined, which was related to the generalized projections in the Fourier transform domain. It was shown that, by applying a time-invariant filter to $U_B(\underline{x})$, we can obtain an image, $U_R(\underline{x})$, which in the Fourier domain is a linear combination of the velocity and density scattering potentials, and where the coefficients depend on the angle of incidence of the probing wave. Therefore, for numerical stability, several angles of incidence were used to solve for the velocity and density scattering potentials separately.

## Acknowledgements

This work was supported by the Air Force Office of Scientific Research under Grant No. AFOSR-85-0227, by the National Science Foundation under Grant No. ECS-83-12921, and by the Vertical Seismic Profiling Consortium at the MIT Earth Resources Laboratory.

## References

C. Esmersoy and D. Miller, "Stacking Versus Back Propagation in Seismic Imaging: Duality for Multidimensional Linearized Inversion," presented at the 57th Ann. Int. Mtg. and Expos., Soc. Explor. Geophys., New Orleans, Expanded Abstracts, pp. 744–746, Oct. 1987.

J. A. Fawcett, "Inversion of N-Dimensional Spherical Averages," *SIAM J. Appl. Math.*, Vol. 45, No. 2, pp. 336–341, April 1985.

A. Özbek and B. C. Levy, "Inversion of Parabolic and Paraboloidal Projections," submitted to *IEEE Trans. Acoust. Speech Signal Processing*, April 1987.

A. Özbek and B. C. Levy, "Simultaneous Inversion of Velocity and Density Profiles for Multidimensional Acoustic Media," submitted to *J. Acoust. Soc. Am.*, May 1988.

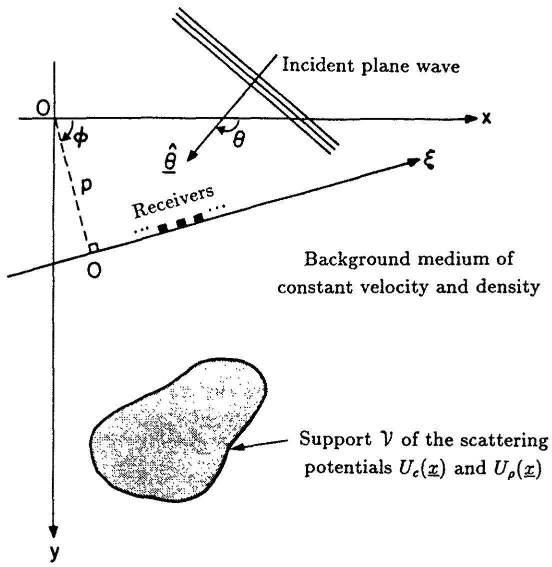


FIG. 1. 2-D experimental geometry.

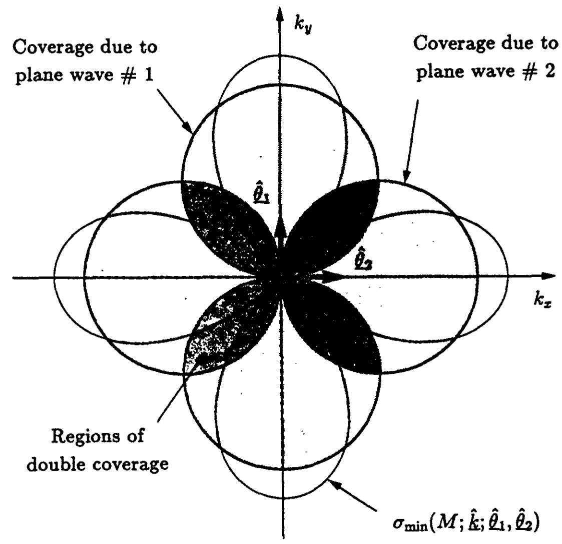


FIG. 2. Frequency coverage of $\hat{U}_R(k)$ and the "radiation pattern" of $\sigma_{min}$ (M;$\hat{k}$;$\hat{\theta}_1$, $\hat{\theta}_2$).

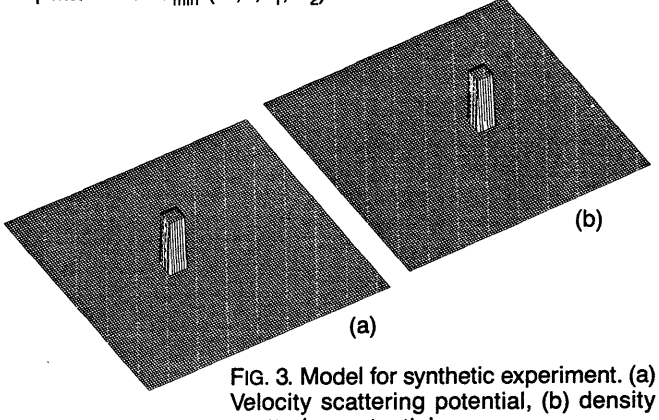


FIG. 3. Model for synthetic experiment. (a) Velocity scattering potential, (b) density scattering potential.

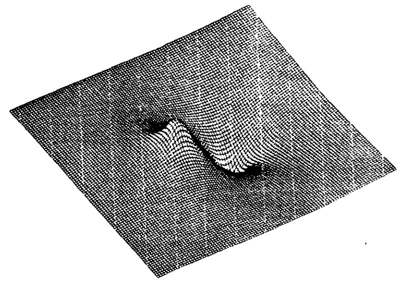

FIG. 4. Backprojected image, obtained assuming a constant density medium.

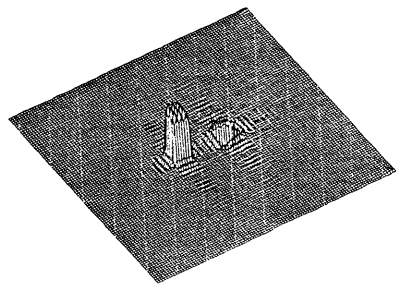

FIG. 5. Inverted image, obtained assuming a constant density medium.

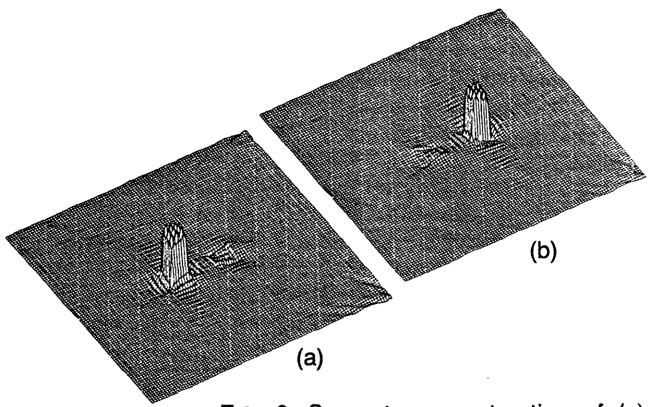


FIG. 6. Separate reconstruction of (a) velocity scattering potential, and (b) density scattering potential.